Available online at www.sciencedirect.com
SCIENCE DIRECT®
Diamond and Related Materials 12 (2003) 1453–1459
DIAMOND AND RELATED MATERIALS
www.elsevier.com/locate/diamond

Growth and field emission of carbon nanofibers on electroless Ni–P alloy catalyst

Ting-Kan Tsai[a,b,*], Chia-Chih Chuang[c], Chuen-Guang Chao[a], Wei-Long Liu[b]

[a]*Department of Materials Science and Engineering, National Chiao Tung University, Hsinchu 300, Taiwan, ROC*
[b]*Department of Materials Science and Engineering, National Huwei Institute of Technology, Huwei, Yunlin 632, Taiwan, ROC*
[c]*Department of Materials Science and Engineering, National Tsing Hua University, Hsinchu 300, Taiwan, ROC*

Received 17 July 2002; received in revised form 15 April 2003; accepted 21 April 2003

Abstract

Carbon nanofibers (CNFs) were grown on a Ni–P alloy catalyst deposited on a silicon substrate in a microwave heating chemical vapor deposition system with methane gas at 650 °C. The Ni–P alloy catalyst films with various thicknesses were produced using an electroless plating nickel technique. The nanosized clusters on the clustered surface of the Ni–P alloy catalyst film directly provided the nucleation sites for CNFs without any pretreatment before the growth of the CNFs. The CNFs grown on the Ni–P alloy catalyst showed random orientation and it composed of parallel graphite planes with defects tilted from their axis. Field emission measurement indicated that the Ni–P catalyzed-CNFs exhibited excellent field emission properties. The diameter, growth rate and field emission properties show a strong correlation with the thickness of the Ni–P alloy catalyst film.

Keywords: Carbon nanofibers; Chemical vapor deposition; Field emission; Ni–P alloy

1. Introduction

Carbon nanofibers (CNFs), sometimes known as carbon filaments, are one kind of carbon nanostructure. This kind of carbon nanostructure is clearly distinguished from carbon nanotubes (CNTs) in structural conformation, although they often show great resemblance in morphology. CNFs generally show a similar fullerence-like tip but with much disorder in the graphite crystallization all along the fiber [1]. In contrast, the CNTs have well-ordered graphite crystallinity [2]. Through careful control of the synthetic conditions including the chemical nature and physical conformation of catalyst, the composition and flow rate of hydrocarbon gas reactant and reaction temperature, assorted CNF structures with various morphologies and different degrees of crystallinity can be produced [3]. CNFs growth on metal catalyst particles such as Fe, Co, Ni and their alloys from the decomposition of hydrocarbons have been known for a very long time [4–9]. In more recent years, vapor growth carbon fibers have attracted much attention, due to their extraordinary physical and chemical properties [10–12]. Efforts have been made to control the morphology and property of CNFs and improve the efficiency of the production processes [2,13–18].

Chemical vapor deposition (CVD) has been widely used for CNTs, CNFs and other carbon nanostructures synthesis due to its high product yield and scale up capability. In the CVD method, the catalyst plays an important and indispensable role for the growth of CNFs. Chemical composition and particle size of the catalyst determine the structure, property and diameter of the CNFs. Many investigations have been developed to prepare the catalyst for depositing CNFs. Merkulov et al. [16] evaporated Ni on (0 0 1) n-type Si by e-gun. Shyu and Hong [17] deposited Fe–Ni with various components by e-beam evaporation. Chen et al. [18] reduced foam Ni in flowing H_2 at 300 °C and transformed it into a thin slice shape prior to the creation of the CNFs. Baker et al. [7] prepared copper–nickel powder by coprecipitation of the metal carbonates from

*Corresponding author. Tel.: +886-5-632-9643x621; fax: +886-5-636-1981.
E-mail address: dktsai@sunws.nhit.edu.tw (T.-K. Tsai).

0925-9635/03/$ - see front matter © 2003 Elsevier Science B.V. All rights reserved.
doi:10.1016/S0925-9635(03)00173-0

Table 1
The composition of plating solution and the experimental condition for electroless Ni–P plating

Chemicals	Concentration (g/l)
$NiSO_4 \cdot 6H_2O$	20
$NaH_2PO_2 \cdot H_2O$	27
$Na_2C_4H_4O_4 \cdot 6H_2O$	16
$Pb(NO_3)_2$	1 ppm
pH 4.2	Temperature 70 °C

mixed nitrate solutions using ammonium bicarbonate and a sequence complex treatment process including drying, calcining and reducing, etc. These methods need expensive equipment or complex processes for depositing the metal catalyst film and for clustering the metal catalyst film to nanoparticles.

The electroless plating nickel technique is a simple process with low cost and is easy to manage. This technique has been applied for ohmic contacts to silicon in semiconductor devices and for contact filling in very large scale integrated [19] for several years. However, there is little literature mentioned about electroless plating Ni deposited on substrates for fabricating CNFs. In this paper, we have deposited Ni–P alloy as catalyst on a silicon substrate using the electroless plating technique and a systematic study of the growth morphology and field emission property of CNFs from methane using Ni–P alloy catalyst in a microwave heating CVD system.

2. Experimental

A Ni–P alloy catalyst film was deposited using the electroless plating technique on a p-type (1 0 0) silicon wafer (resistivity ~1–20 Ω cm). Prior to the electroless plating process, it is necessary to sensitize and activate the surface of silicon wafer using $SnCl_2$ and $PdCl_2$ solutions. The plating solution was composed of a mixture of $NiSO_4$, NaH_2PO_2, $Na_2C_4H_4O_4$ and $Pb(NO_3)_2$, where $NiSO_4$ as the main nickel source, NaH_2PO_2 is the reducing agent, $Pb(NO_3)_2$ is the stabilizing agent, and $Na_2C_4H_4O_4$ is the buffer and complex agent for nickel. Since NaH_2PO_2 was used as a reducer, the electroless plated nickel structures always incorporated with phosphorus. The composition of the plating solutions and the experimental conditions are listed in Table 1. Thin Ni–P alloy catalyst films with various thickness were deposited onto the wafers for 10, 15 and 20 s.

A microwave heating CVD system has been utilized for growth of CNFs. The electroless Ni–P deposited-silicon substrate was placed on a ceramic holder, which was heated up to approximately 650 °C by controlling the microwave power. The temperature was detected by a thermocouple contacted to the ceramic holder. CNFs were grown on the substrate using methane gas as the source of carbon with flow rate 200 cc/min. The pressure of the chamber was kept at atmosphere.

Transmission electron microscopy (TEM) was utilized to observe the cross-sectional images of Ni–P alloy catalyst films and atomic force microscopy (AFM) was used to observe the surface morphology of the Ni–P alloy catalyst films. The morphology of the CNFs film deposited on the substrate was observed by field emission scanning electron microscopy. The structure of the CNFs was characterized by high-resolution transmission electron microscopy (HRTEM). Raman spectroscopy was used to confirm the formation of graphitized CNFs. Field emission properties were measured by taking electron emission current density–electric field (I–V) curves using a Keithley 237 in a vacuum (10^{-6} Torr) chamber at room temperature. A voltage up to 1100 V was applied and the distance between the indium–tin oxide film and the CNF's tip is 180 μm.

3. Results and discussion

3.1. The morphology of the electroless Ni–P alloy catalyst film

Fig. 1 is a TEM cross-section image of the electroless Ni–P alloy catalyst film. The thickness of Ni–P alloy catalyst film, in Fig. 1a–c, was measured to be approximately 20, 30 and 40 nm in samples deposited for 10, 15 and 20 s, respectively. These samples with 20, 30 and 40 nm catalyst films are designated as sample A, sample B and sample C, respectively. It is clear that the thickness of the deposited catalyst film increases with the deposition time. When the deposition duration is extended, the Ni–P alloy catalyst film became dense from sparse and the surface of catalyst film became flatter gradually.

Fig. 2 is the AFM surface morphology image of the Ni–P alloy catalyst films. Fig. 2a–c show the surface morphologies of sample A, sample B and sample C, respectively. These figures show clearly that the clustered surface of the electroless Ni–P alloy catalyst film with different thickness consists of Ni–P alloy clusters with different size. When the deposited thickness is increased, the size of clusters is increased and the morphology of the clustered surface gradually becomes dense. The size of clusters in sample A, sample B and sample C are approximately 12–30, 26–37 and 35–42 nm, respectively. These nanosized clusters will directly provide the nucleation sites for CNFs without any pretreatment for catalyst film.

These above-mentioned results from TEM cross-section images and AFM surface morphology images indicate that the clustered surface morphology of the

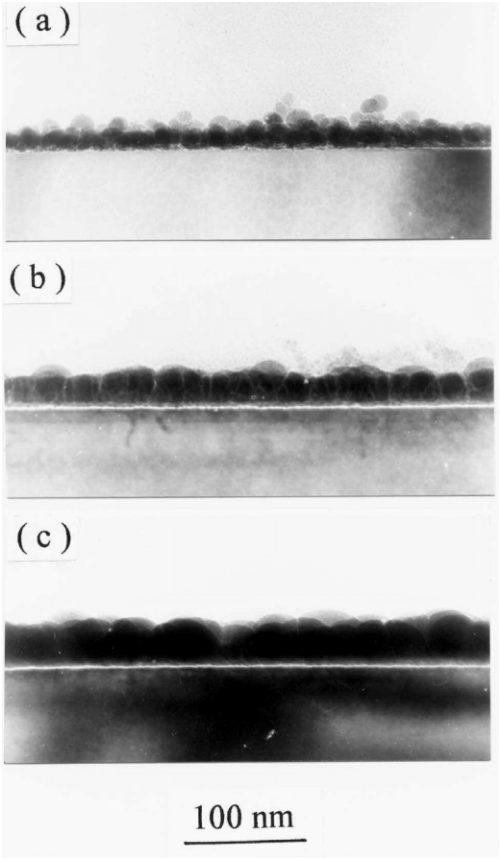

Fig. 1. TEM cross-section images of the electroless Ni–P alloy catalyst film with various thicknesses. (a) Sample A was deposited for 10 s; (b) sample B was deposited for 15 s and (c) sample C was deposited for 20 s.

electroless Ni–P alloy catalyst film is relevant to its thickness. The morphology of the catalyst film is known to play a critical role in CNF growth. So, the thickness of the Ni–P alloy catalyst film will affect the growth and the property of CNFs.

3.2. The growth of CNFs

Fig. 3 shows scanning electron microscopy (SEM) images of CNFs grown at substrate temperature approximately 650 °C for 7 min. Fig. 3a–c illustrate the growth behavior of CNFs in sample A, sample B and sample C, respectively. It reveals that the growth rate of CNFs is related to the thickness of Ni–P alloy catalyst film. Fig. 3a illustrates that the sample A with approximately 20 nm thick catalyst film is completely covered with CNFs. With increasing catalyst film thickness (Fig. 3b and c), the amount of CNFs clearly decreases. In Fig. 3c, the thickness of catalyst film is approximately 40 nm. Only a few CNFs appear on the surface of substrate and many catalyst clusters are observed. The results indicate that the growth rate of the CNFs decreases as the thickness of the catalyst film increases. Our results agree with those obtained by Wei et al. [20]. They have synthesized multiwall CNTs by thermal CVD using Ni and Fe catalyst films with various thicknesses.

The phenomenon stated above can be explained by the diffusion of carbon atom into the catalyst particle. The growth of carbon nanostructures, including CNTs and CNFs, occurs by diffusion driven precipitation of carbon atoms from the supersaturated catalyst particles [3,4]. The size of catalyst particle increases and that causes the diffusion length to increase and the gradient of supersaturation to decrease. These factors will decrease the growth rate of CNFs. So, the thin catalyst film has a larger growth rate than the thick catalyst film. The result also proves that diffusion of carbon through the catalyst particle is the rate-determining step in the growth of carbon nanostructures using a Ni–P alloy catalyst.

Fig. 4 is the SEM micrograph showing the surface morphology of CNFs grown at approximately 650 °C for 10 min. Fig. 4a–c correspond to sample A, sample B and sample C, respectively. All of these SEM images show that these CNFs grown on the catalyst film with various thicknesses have similar morphology and are not vertically aligned but randomly tangled. A more noteworthy characteristic is the catalyst film thickness that affect on the diameter of the CNFs. The diameter of the CNFs in Fig. 4a–c is approximately 30–70, 50–120 and 70–150 nm, respectively. The diameter of the CNFs increases as the size of the catalyst clusters increases with catalyst film thickness. The results show that the diameter of the CNFs is dependent on the initial

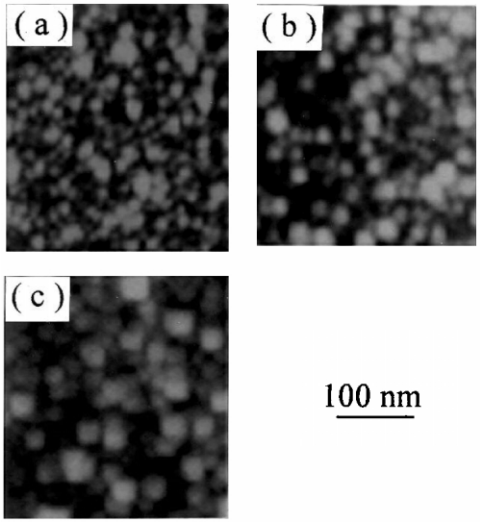

Fig. 2. AFM surface morphology images of the electroless Ni–P alloy catalyst film with different size of clusters. (a) Sample A was deposited for 10 s; (b) sample B was deposited for 15 s and (c) sample C was deposited for 20 s.

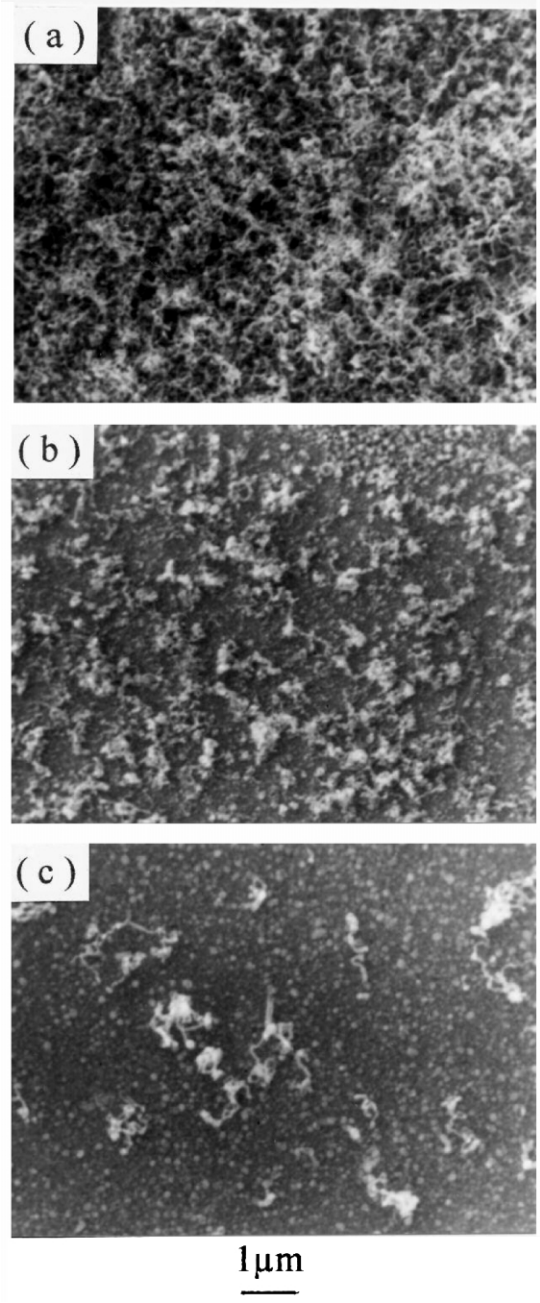

Fig. 3. SEM images of CNFs grown at substrate temperature approximately 650 °C for 7 min. The corresponding thickness of Ni–P alloy catalyst film is 20, 30 and 40 nm in images (a), (b) and (c), respectively.

thickness of predeposited catalyst film. Wei et al. [20], Yudasaka et al. [21] and Bower et al. [22] in their reports using Fe, Co and Ni catalyst film also agree on this point.

3.3. Structural analysis

Raman spectroscopy has been extensively used to characterize various carbon materials. This technique shows a high sensitivity for identifying carbon nanostructures due to the matching of the energy of the incident photon and strong optical absorption–electronic transitions of carbon nanostructures [23]. For the interpretation and evaluation of grown CNFs, each peak should be confirmed on the basis of the previously reported Raman measurements of carbon nanostructures. There are only two obvious peaks in Raman spectra for all samples with various thicknesses, as shown in Fig. 5. The peak of the G mode located at approximately 1599/cm, suggesting that the carbon nanostructures are multiwalled tubes or fibers with crystalline graphitic

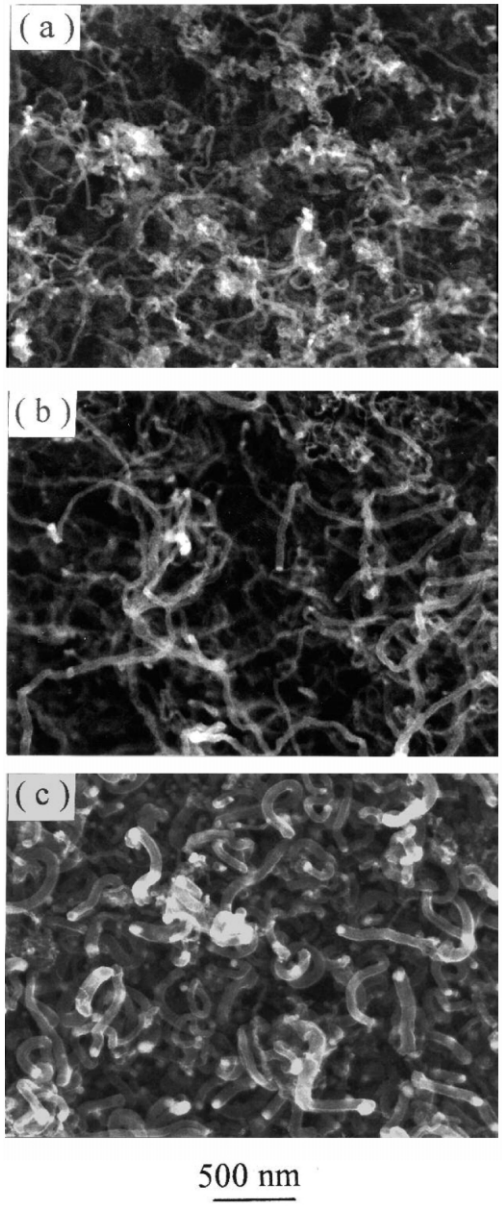

Fig. 4. SEM images of CNFs grown at substrate temperature approximately 650 °C for 10 min. The corresponding thickness of Ni–P alloy catalyst film is 20, 30 and 40 nm in images (a), (b) and (c), respectively.

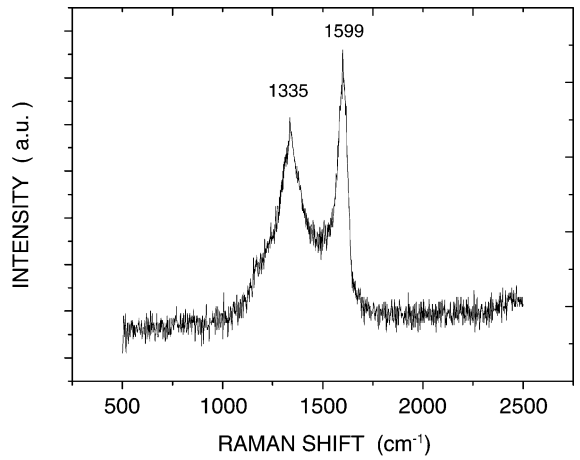

Fig. 5. Raman spectrum for CNFs grown on the Ni–P alloy catalyst at substrate temperature approximately 650 °C for 10 min.

sheets. The peak which originates from finite size effects or lattice distortions located at approximately 1335/cm (D mode) is also observed, indicating the existence of amorphous carbonaceous particles and defective graphite layers in the wall. The Raman spectra reveal that CNFs have a multiwalled structure with defective graphite sheets in the wall.

HRTEM was used to investigate and characterize the structure of CNFs. Fig. 6 is the HRTEM observation of the CNFs growth on sample B. The HRTEM image reveals that the CNFs are composed of parallel graphite planes tilted from their axis and have many defects in the tube wall. Sample A and sample C have the same structural characteristic as sample B. This result is consistent with the above observation of Raman spectrum. The defects in the fiber wall cause the distortion of graphite plane and are reflected in the widening of the peak of the D mode.

3.4. Electron emission measurement

Fig. 7 illustrates the electron emission current density vs. electric field (I–V) curves of CNFs. Curve (a) to curve (c) in Fig. 7 give the I–V data from the CNFs grown on sample A, sample B and sample C, respectively. For sample A, the turn-on field was approximately 0.11 V/μm with an emission current density of 10 μA/cm^2 and the threshold field was 3.1 V/μm with an emission current density of 10 mA/cm^2. Sample B and sample C have almost the same turn-on field approximately 0.22 V/μm, but the threshold field is 3.4 and 4.1 V/μm, respectively. These results show that all CNFs exhibit outstanding emission properties including a low onset electrical field and high emission current densities. The inset in Fig. 7 shows Fowler–Norheim (F–N) plots of the same emission data. The plot of $\ln|I/V|$ vs. $|I/V|$ is approximately a straight line,

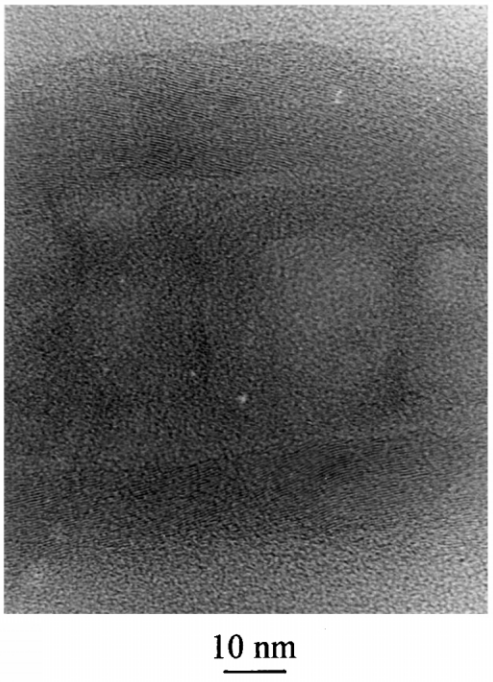

Fig. 6. High-resolution TEM image of CNFs grown on the Ni–P alloy catalyst at substrate temperature approximately 650 °C for 10 min.

indicating that the emitted electrons mainly follow the field emission process.

The field emission character of the CNFs is determined by the intrinsic structure, chemical properties, aligned density and orientation of the nanofibers. However, there is a lack of fundamental understanding of the mechanism responsible for the electron emission from carbon-based materials. The excellent field emission properties of Ni–P alloy catalyzed-CNFs may be

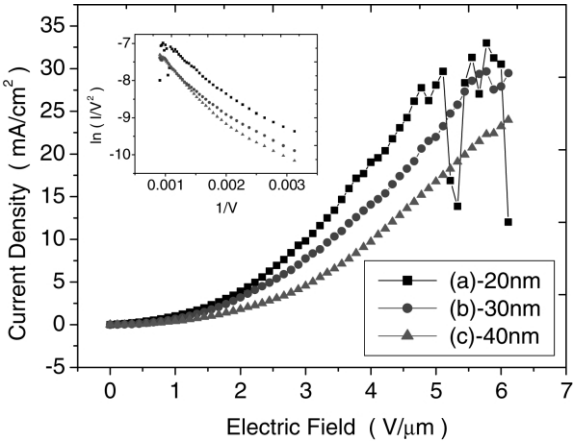

Fig. 7. Field emission current density vs. electric field curves for CNFs. From curve (a) to (c), the thickness of Ni–P alloy catalyst film corresponds to 20, 30 and 40 nm. *Inset:* Corresponding Fowler–Nordheim plot.

attributed to the random orientation (as seen in Fig. 4) and defects (as seen in Fig. 6) of CNFs. Davydov et al. [24] have also pointed out that perfectly aligned CNTs were less efficient field emitters and had lower field enhancement than chaotic CNTs. Meanwhile, Groning et al. [25] also suggested that some random CNTs exhibited better field emission properties than the aligned CNTs. These results keep confirming to our supposition. Another reason for the excellent field emission properties is the defect effect. Some reports relating defect densities to field emission properties have also been proposed [26,27]. The enhanced emission may originate from the defect-induced energy bands that are formed within the band gap of graphite. The energy barrier that the electrons must tunnel through to be emitted is reduced, so the electrons residing at these defect levels can be emitted directly into vacuum from these bands or be transported to the surface states for emission [28]. Chen et al. [29], in their research on field emission of different oriented CNTs, discovered that the CNTs oriented parallel to the substrate have a lower onset applied field than those oriented perpendicular to the substrate. They also suggested that the defect emission mechanism is a reason for the low onset electrical field. Obraztsov et al. [30] have also found that the field emission properties were improved by increasing the density of structural defects.

Fig. 7 also indicates that the field emission properties of CNFs with small diameter are better than those of the CNFs with large diameter. Conventional field emission analysis for carbon nanostructures utilizes the F–N equation, which can be written in terms of experimentally measured quantities as

$$\ln\left|I/V^2\right| = (B\Phi^{3/2}d/\beta)/V + \text{offset}.$$

where I is the total current, V is the applied voltage, d is the distance between cathode and anode, β is the field enhancement factor, Φ is the emitter work function and B is equal to -6.83×10^9 $(\mathrm{V}/(\mathrm{eV}^{3/2}\,\mathrm{m}))$. The slope S (i.e. $B\Phi^{3/2}d/\beta$) of the F–N plot obtained from the experimental data is a constant and directly reflects field emission properties. Here, d is an experimental parameter, B is a constant, and only Φ and β are related to the properties and structure of carbon nanostructures. An in-depth study on Φ and B for CNTs was made by Zhou et al. [31]. Their study revealed that Φ slightly increases and β gradually decreases with increasing tube diameter. The result completely supports our experimental observation.

A clear fluctuation of the I–V curve at higher voltages for CNFs is seen in Fig. 7, indicating some emission sites are damaged or destroyed. In particular, this phenomenon is obvious for CNFs with small diameter as in sample A. It is reasonable to suggest that the CNFs with small diameter are more easily damaged by ion bombardment than the CNFs with large diameter [32].

4. Conclusion

In this present study, an electroless nickel plating technique was used to deposit Ni–P alloy catalyst film for CNFs growth from methane in a microwave heating CVD system at 650 °C. The nanosized clusters on the clustered surface of Ni–P alloy catalyst film will directly provide the nucleation sites for CNFs without any pretreatment for catalyst film. The CNFs grown on Ni–P alloy catalyst shows random orientation for all samples with various thicknesses, but the diameter variation and the growth rate were clearly dependent on the initial thickness of catalyst film. Raman spectrum and HRTEM observations revealed that the multiwalled CNFs are composed of parallel graphite planes tilted from their axis and have many defects in the wall. Field emission measurements indicated that the CNFs with random orientation and many defects exhibited excellent field emission properties. The CNFs with small diameter has better field emission properties than the CNFs with large diameter, but were easily damaged by ion bombardment.

Acknowledgments

The authors gratefully acknowledge research assistance by Wen-Jauh Chen and Shu-Hue Hsieh.

References

[1] A.M. Bonnot, M.N. Séméria, J.F. Boronat, T. Fournier, L. Pontonnier, Diamond Relat. Mater. 9 (2000) 852.
[2] V.I. Merkulov, D.H. Lowndes, Y.Y. Wei, G. Eres, E. Voelkl, Appl. Phys. Lett. 76 (2000) 3555.
[3] N.M. Rodriguez, J. Mater. Res. 8 (1993) 3233.
[4] R.T.K. Baker, M.A. Barber, P.S. Harris, F.S. Feates, R.J. Waite, J. Catal. 26 (1972) 51.
[5] R.T.K. Baker, P.S. Harris, R.B. Thomas, R.J. Waite, J. Catal. 30 (1973) 86.
[6] R.T.K. Baker, Carbon 27 (1989) 315.
[7] M.S. Kin, N.M. Rodriguez, R.T.K. Baker, J. Catal. 131 (1991) 60.
[8] Y. Li, J. Chen, L. Chang, Y. Qin, J. Catal. 178 (1998) 76.
[9] Z. Li, J. Chen, X. Zhang, Y. Li, K.K. Fung, Carbon 40 (2002) 409.
[10] M. Ishioka, T. Okada, K. Matsubara, M. Endo, Carbon 30 (1992) 859.
[11] G.G. Tibbetts, Carbon 30 (1992) 1399.
[12] T. Masuda, S.R. Mukai, K. Hashimoto, Carbon 30 (1992) 124.
[13] Y. Chen, S. Patel, Y. Ye, D.T. Shaw, L. Guo, Appl. Phys. Lett. 73 (1998) 2119.
[14] K.B.K. Teo, M. Chhowalla, G.A.J. Amaratunga, et al., Appl. Phys. Lett. 80 (2002) 2011.
[15] M. Endo, Y.A. Kim, T. Hayashi, et al., Appl. Phys. Lett. 80 (2002) 1267.
[16] V.I. Merkulov, A.V. Melechko, M.A. Guillorn, D.H. Lowndes, M.L. Simpson, Appl. Phys. Lett. 80 (2002) 476.

[17] Y.M. Shyu, F.C.N. Hong, Diamond Relat. Mater. 10 (2001) 1241.
[18] X.H. Chen, J.X. Wang, H.S. Yang, G.T. Wu, X.B. Zhang, W.Z. Li, Diamond Relat. Mater. 10 (2001) 2057.
[19] C.H. Ting, H. Paunovic, J. Electrochem. Soc. 136 (1989) 456.
[20] Y.Y. Wei, G. Eres, V.I. Merkulov, D.H. Lowndes, Appl. Phys. Lett. 78 (2001) 1394.
[21] M. Yudasaka, R. Kikuchi, T. Matsui, Y. Ohki, S. Yoshimura, E. Ota, Appl. Phys. Lett. 67 (1995) 2477.
[22] C. Bower, O. Zhou, W. Zhu, D.J. Werder, S. Jin, Appl. Phys. Lett. 77 (2000) 2767.
[23] Y.H. Mo, A.K.M.F. Kibria, K.S. Nahm, Synthetic Met. 122 (2001) 443.
[24] D.N. Davydov, P.A. Sattari, D. AlMawlawi, A. Osika, T.L. Haslett, J. Appl. Phys. 86 (1999) 3983.
[25] O. Groning, O.M. Kuttle, C. Emmenegger, P. Groning, L. Shlapbach, J. Vac. Sci. Technol. B 18 (2000) 665.
[26] C. Wang, A. Garcia, D.C. Ingram, M. Lake, M.E. Kordesch, Electron. Lett. 27 (1991) 1459.
[27] N.S. Xu, R.V. Latham, Y. Tzeng, Electron. Lett. 29 (1993) 1596.
[28] W. Zhu, C. Bower, G.P. Kochanski, S. Jin, Solid-State Electron. 45 (2001) 921.
[29] Y. Chen, D.T. Shaw, L. Guo, Appl. Phys. Lett. 76 (2000) 2469.
[30] A.N. Obraztsov, I.Y. Pavlovsky, A.P. Volkov, et al., Diamond Relat. Mater. 8 (1999) 814.
[31] G. Zhou, W. Duan, B. Gu, Appl. Phys. Lett. 79 (2001) 836.
[32] J.-M. Bonard, J.-P. Salvetat, T. Stöckli, W.A. de Heer, L. Forró, A. Châtelain, Appl. Phys. Lett. 73 (1998) 918.